Received: 28 February 2020 | Accepted: 8 September 2020

DOI: 10.1111/jth.15110

ORIGINAL ARTICLE

Hydrogen sulfide-loaded microbubbles combined with ultrasound mediate thrombolysis and simultaneously mitigate ischemia-reperfusion injury in a rat hindlimb model

Jiayuan Zhong[1,2,3,4] | Yili Sun[1,3,4] | Yuan Han[1,3,4] | Xiaoqiang Chen[1] | Hairui Li[1,5] | Yusheng Ma[1] | Yanxian Lai[1] | Guoquan Wei[1] | Xiang He[1] | Mengsha Li[1] | Wangjun Liao[6] | Yulin Liao[1] | Shiping Cao[1,3,4] | Jianping Bin[1,3,4]

[1]Department of Cardiology, State Key Laboratory of Organ Failure Research, Nanfang Hospital, Southern Medical University, Guangzhou, China

[2]Department of Cardiology, Liuzhou People's Hospital, Liuzhou, China

[3]Guangzhou Regenerative Medicine and Health Guangdong Laboratory, Guangzhou, China

[4]Guangdong Provincial Key Laboratory of Shock and Microcirculation, Guangzhou, China

[5]Department of Cardiology, The First Affiliated Hospital of Jinan University, Guangzhou, China

[6]Department of Oncology, Nanfang Hospital, Southern Medical University, Guangzhou, China

Correspondence
Jianping Bin and Shiping Cao, Department of Cardiology, State Key Laboratory of Organ Failure Research, Nanfang Hospital, Southern Medical University, 1838 Guangzhou Avenue North, Guangzhou 510515, China.
Emails: jianpingbin@hotmail.com; jianpingbin@126.com (JB); csp2012@126.com (SC)

Funding information
This work was supported by the National Natural Science Foundation of China (No. 81571698 and No. 81771857) and Guangzhou regenerative medicine

Abstract

Background: Thromboembolism and subsequent ischemia/reperfusion injury (IRI) remain major clinical challenges.

Objectives: To investigate whether hydrogen sulfide (H_2S)-loaded microbubbles (hs-Mbs) combined with ultrasound (US) radiation (hs-Mbs+US) dissolve thrombi and simultaneously alleviate tissue IRI through local H_2S release.

Methods: hs-Mbs were manufactured and US-triggered H_2S release was recorded. White and red thromboembolisms were established ex vivo and in rats left iliac artery. All subjects randomly received control, US, Mbs+US, or hs-Mbs+US treatment for 30 minutes.

Results: H_2S was released from hs-Mbs+US both ex vivo and in vivo. Compared with control and US, hs-Mbs+US and Mbs+US showed comparable substantial decreases in thrombotic area, clot mass, and flow velocity increases for both ex vivo macrothrombi. In vivo, hs-Mbs+US and Mbs+US caused similarly increased recanalization rates, blood flow velocities, and hindlimb perfusion for both thrombi compared with the other treatments, with no obvious influence on hemodynamics, respiration, and macrophage vitality. More importantly, hs-Mbs+US substantially alleviated skeletal muscle IRI by reducing reactive oxygen species, cellular apoptosis, and proapoptotic Bax, caspase-3, and caspase-9 and increasing antiapoptotic Bcl-2 compared with other treatments. In vitro, hypoxia/reoxygenation-predisposed skeletal muscle cells and endothelial cells treated with normal saline solution exhibited similar trends, which were largely reversed by an H_2S scavenger or an inhibitor of Akt phosphorylation.

J.Z., Y.S., and Y.H. contributed equally to this work.

This work was carried out in Department of Cardiology, State Key Laboratory of Organ Failure Research, Nanfang Hospital, Southern Medical University, Guangzhou, 510515, China.

Manuscript handled by: Wolfgang Bergmeier

Final decision: Wolfgang Bergmeier and 08 September 2020

and Health Laboratory of Guangdong (2018GZR110105009).

Conclusion: hs-Mbs+US effectively dissolved both white and red macrothrombi and simultaneously alleviated skeletal muscle IRI through the US-triggered, organ-specific release of H_2S. This integrated therapeutic strategy holds promise for treating thromboembolic diseases and subsequent IRI.

KEYWORDS
hydrogen sulfide, ischemia/reperfusion injury, microbubbles, thrombolysis, ultrasound

1 | INTRODUCTION

Thromboembolic diseases such as myocardial infarction and stroke are prevalent worldwide and associated with high disability and mortality rates.[1] Rapid restoration of blood flow by vascular recanalization is essential in thromboembolism treatment.[2,3] Current conventional strategies to recanalize an occluded vessel are catheter intervention and thrombolytic agent perfusion, which have contributed to substantial improvements in the salvage of endangered tissue and long-term patient outcomes. However, despite rapid reperfusion by any of these strategies, paradoxical organ injury, referred to as ischemia/reperfusion injury (IRI), accompanies the restoration of blood flow and concomitant reoxygenation.[4] IRI triggers further organ damage, such as myocardial arrhythmia and stunning, microvascular obstruction and lethal IRI, which decrease the benefits of recanalization and cause further deterioration, with increased disability and mortality, through various mechanisms involving oxidative stress (OS), mitochondrial dysfunction, and cell apoptosis.[5] Myocardial IRI is reportedly responsible for up to 50% of the final infarct size.[6]

Over the decades, there have been considerable efforts to address IRI, and some promising results have been obtained in animal studies. However, currently, there are no satisfactory therapies for treating IRI in clinical practice.[7,8] The results of clinical studies investigating pharmacologic agents have been mixed,[9] and no drugs have been designed to specifically target organs affected by IRI, thus decreasing the adverse effects of the drug. Although ischemic conditioning strategies are promising, the effects are weak and, in some cases, inconsistent.[10] More importantly, in urgent IRI situations such as primary percutaneous coronary intervention, the procedure of ischemic preconditioning may delay the time to vessel recanalization.

Hydrogen sulfide (H_2S), a biological gas that is widespread in the body, is emerging as an attractive strategy for IRI treatment. Accumulating evidence indicates that H_2S is protective against IRI in the animal heart, liver, kidney, lung, and brain through multifaceted mechanisms.[11-15] However, challenges exist in achieving low toxicity and long-term activity and ensuring the specific bioavailability of H_2S to injured tissue. In most studies, H_2S was delivered systemically as a gas or in a donor such as normal saline (NaHS) and Na_2S, which are not ideal sources of H_2S; they cause a drastic increase in blood H_2S levels, which has systemic side effects, and contribute to the short persistence of H_2S in blood and the mediocre availability to target tissues, crippling the therapeutic potency of H_2S in target organs.[16,17] More recently studied long-lasting H_2S compounds, such as diallyl trisulfide and SG-1002, are released more slowly,[18,19] but they may not fix the problem of nonspecific H_2S delivery to endangered tissue. An organ-specific H_2S delivery system may address the therapeutic challenges.

Essentials

- Thromboembolism and subsequent ischemia/reperfusion injury remain major clinical challenges.
- White and red thromboembolisms were established ex vivo and in rats left iliac artery.
- hs-Mbs+US effectively dissolves macrothrombi and alleviates skeletal muscle IRI by H_2S release.
- hs-Mbs+US holds promise for treating thromboembolic diseases and subsequent IRI.

Currently, ultrasound-treated microbubbles (Mbs+US) are a valuable tool for the organ-specific delivery of drugs, gases, or genes.[20] In response to regional acoustic pressure, Mbs oscillate and finally collapse (cavitation) to locally release cargo, diminishing unwanted systemic side effects. It has been reported that the delivery of nitric oxide and oxygen by Mbs+US is feasible and beneficial for treating myocardial infarction and destroying tumor neovasculature, respectively.[21,22] Our previous work demonstrated that US+Mbs carrying H_2S (hs-Mbs+US) can specifically release H_2S at the myocardium and attenuate rat myocardial IRI without obvious systemic side effects.[23]

Through US-induced Mbs cavitation, Mbs+US are also emerging as an attractive and effective adjunct to current recanalization strategies such as vascular intervention and thrombolytic drugs when patients are too weak to undergo an operation, are at high risk of bleeding or show the no-reflow phenomenon that sometimes follows large vessel recanalization. Evidence shows that Mbs+US are efficacious at lysing acute macrothrombi in iliofemoral, coronary, and carotid arteries, thus improving organ perfusion and outcomes in animals.[24-28] In addition, Mbs+US effectively dissolved microthrombi in the brain and heart and improved organ function in a mouse acute ischemic stroke model and a canine coronary no-reflow model, respectively.[29,30] Thus, given that Mbs+US can boost thrombolysis, US+hs-Mbs holds great promise as an

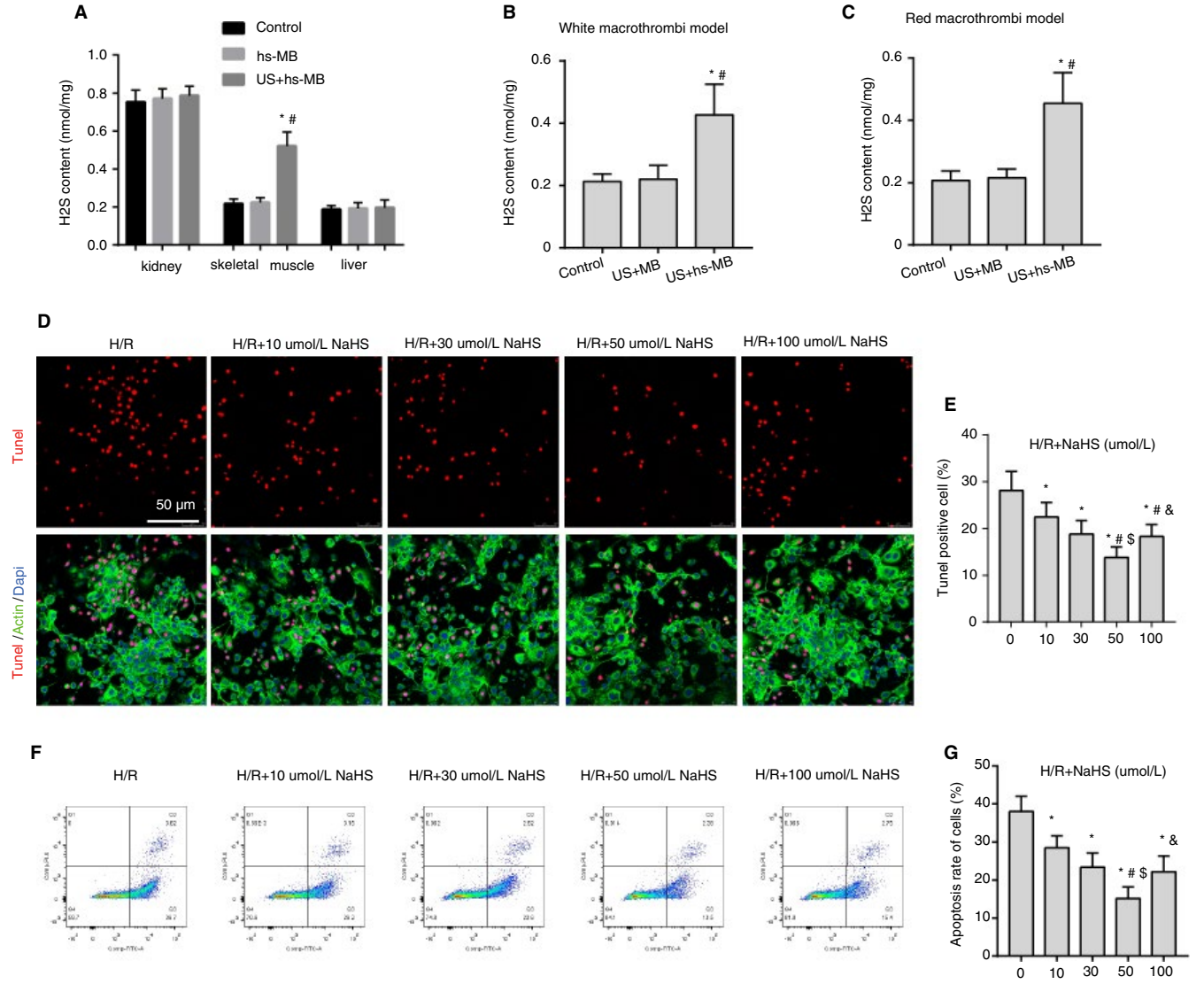

FIGURE 1 Ultrasound-triggered H_2S release from hs-Mbs to tissues. (A) H_2S content in various tissues in nonthromboembolized rats immediately after US+hs-MB treatment (n = 3). *P < .05 vs control; #P < .05 vs hs-MB.H_2S content in hindlimb skeletal muscle immediately after treatments in (B) white and (C) red left iliac artery-thromboembolized rats (n = 6). *P < .05 vs control; #P < .05 vs US+MB. Representative (D) pictures and (E) quantification of L6 cell sections stained with TUNEL. (F) Evaluation of cellular apoptosis by Comp-FITC-A/Comp-PI A double staining and flow cytometry. (G) Quantification. *P < .05 vs 0 μmol/L NaHS; #P < .05 vs 10 μmol/L NaHS; $$P$ < .05 vs 30 μmol/L NaHS; &P < .05 vs 50 μmol/L NaHS. Control, saline infusion; hs-MB, microbubble loaded with hydrogen sulfide; US, ultrasound; H/R, hypoxia for 2 h with subsequent reoxygenation for 12 h; H/R+NaHS, hypoxia for 2 h followed by immediate addition of NaHS solution, then reoxygenation for 12 h [Color figure can be viewed at wileyonlinelibrary.com]

integrated treatment to achieve prompt thrombosis and simultaneous IRI protection.

In this study, we hypothesized that H_2S-loaded Mbs (hs-Mbs) combined with US radiation (hs-Mbs+US) are thrombolytic and protect against skeletal muscle IRI through local H_2S delivery. We prepared hs-Mbs and detected H_2S release and transit to tissue upon US-triggered hs-Mbs destruction. We also evaluated the lytic efficiency of hs-Mbs+US in vitro and in a rat model of hindlimb macrothrombosis. Furthermore, we investigated the protective effect of hs-Mbs+US against IRI in vivo and explored the underlying mechanism.

2 | METHODS

2.1 | Experimental animals

Male Sprague-Dawley rats weighing 250 to 300 g was supplied by the Laboratory Animal Centre of Southern Medical University. The animal care and experimental protocols followed the guidelines approved by the Institutional Animal Care and Use Committee at Southern Medical University and were in accordance with the National Institutes of Health guidelines.

2.2 | Preparation of Mbs and hs-Mbs

The methods of Mbs and hs-Mbs preparation are described elsewhere.[31] A detailed description is provided in the Appendix S1.

2.3 | Characterization of Mbs and hs-Mbs

The morphology of Mbs and hs-Mbs was characterized by an optical microscope (OLYMPUS BX51, Olympus Optical). The average diameter and concentration of Mb and hs-Mbs in solution were analyzed using a Multisizer III Coulter Counter (Beckman Coulter Inc).

2.4 | In vitro evaluation of US-triggered H_2S release from hs-Mbs

We introduced an artificial flow system to mimic corporeal flow conditions and measure US-triggered H_2S release from hs-Mbs (Figure 1A). Phosphate buffered saline was infused through the system by a peristaltic pump and maintained at a constant flow rate of 10 mL/min. The hs-Mbs suspension was infused into the pipe at a constant 0.01 mL/min. We used a Siemens ultrasonic system and a 4V1c sector-array US transducer (frequency range, 1-4.5 MHz; diameter in azimuthal direction, 32 mm; elevation plane, 5 mm), which was placed 3 cm from the system, and US waves were transmitted through a thick tissue-mimicking phantom to fragment hs-Mbs. The transducer was used in a mechanical index of 1.9 and a frequency of 2 MHz. The H_2S solution concentration was continuously measured by a downstream H_2S-sensitive polarographic electrode connected to a free radical analyzer (TBR4100, World Precision Instruments). The electrode was calibrated to a standard curve derived from an ethylenediaminetetraacetic acid-Na_2S solution in deoxygenated distilled water according to the manufacturer's instructions.[32]

2.5 | In vitro preparation of macrothrombi

Preparation of white and red macrothrombi have been described elsewhere.[33] A detailed description is provided in the Appendix S1.

2.6 | In vitro thrombolysis

The details of the horizontal closed-loop circulating flow system are provided in the Appendix S1. The largely occluded flow in the system was confirmed by B-mode US and pulse-wave Doppler US. Both white and red thrombi were randomly assigned into four treatment groups: control, US, Mbs+US, and US+hs-Mbs groups (n = 15 per group). In the control group, normal saline was infused at a rate of 0.01 mL/min, and the thrombus was left untreated for 30 minutes. In the US group, only US sonication was applied. In the Mbs+US and US+hs-Mbs groups, Mbs or hs-Mbs (1×10^9 Mbs/mL) were infused at a rate of 0.01 mL/min. The transducer of Siemens Acuson Sequoia (4V1c sector-array transducer, frequency: 2 MHz; mechanical index: 1.9; azimuthal plane: 32 mm; elevation plane: 5 mm) was used to sonothrombolysis lengthwise. The treatment lasted for 30 minutes with an intermittent mode of 3 seconds on and 9 seconds off.

2.7 | Left iliac arterial thrombosis model

A description of in vivo white and red macrothrombus preparation is provided in the Appendix S1.

2.8 | In vivo negative and positive control for IRI

Methods of constructing non-thromboembolism-negative control rats and occlusion/recanalization positive control for IRI rats are provided in the Appendix S1.

2.9 | In vivo contrast-enhanced US imaging and in vivo pharmacokinetics of hs-Mbs

A detailed description is provided in the Appendix S1. Rats were infused with Mbs or hs-Mbs (1×10^9 Mbs/mL, 0.01 mL/min) through the jugular vein, and contrast-enhanced US (CEUS) images were acquired to visualize hindlimb blood perfusion when there was a stable distribution of both Mbs. Then, 30 minutes of therapeutic US radiation (mechanical index, 1.9) was used to fragment Mbs or hs-Mbs. Immediately after treatment, hindlimb skeletal muscle, kidney, and liver tissues were collected to detect the H_2S content. The tissues were isolated, homogenized in ice-cold phosphate buffered saline, and centrifuged for 10 minutes at 12 000*g*. The supernatant was collected, and the H_2S concentration was assayed by a TBR4100 free radical analyzer37. MCE 2.7 software (University of Virginia) was used to analyze the perfusion images and video intensity (VI) as previously described.[21]

2.10 | Local in vivo delivery of H_2S by sonication of hs-Mbs and in vivo thrombolysis

The occluded flow in the left iliac artery was confirmed by B-mode US and PW Doppler US. The US was used to destroy Mbs or hs-Mbs for acoustic thrombolysis by a 4V1c sector-array transducer in an oriented lengthwise with vessel flow. White and red thrombi were randomly assigned to four treatment groups: the control, US, Mbs+US, and US+hs-Mbs groups (n = 15 in each group). The control group received an identical amount of normal saline infusion as the other two groups. In the US group, only US sonication was applied. Rats in the Mb+US and hs-Mbs+US groups were infused with Mbs and hs-Mbs suspensions (1×10^9 Mbs/mL), respectively, at a rate of 0.01 mL/min through a polyethylene tube (PE 50) in the right internal jugular vein. Then, rats received US irradiation for 30 minutes. The US transducer was applied

as described for ex vivo thrombolysis. Blood pressure and heart rate were indirectly measured using a blood pressure meter (BP2010AUL, Softron Biotechnology, Ltd.), and the respiratory rate was monitored at 5-minute intervals. Twelve hours after treatment, the hindlimb skeletal muscle was harvested for further analysis.

2.11 | B-Mode and Doppler US imaging

In vitro and in vivo thrombolysis were ultrasonically evaluated, and a description is provided in the Appendix S1.

2.12 | Hindlimb function assessment

At 1 week after the treatment, semiquantitative assessment of impaired hindlimb was performed serially using the "ambulatory impairment score": 3 = dragging of the foot, 2 = no dragging but no plantar flexion, 1 = plantar flexion, and 0 = flexing the toes to resist gentle traction on the tail.

2.13 | Cell culture and treatment

Rat skeletal muscle cells (L6 cells) and human umbilical vein endothelial cells (HUVECs) were maintained in DMEM supplemented with fetal bovine serum (10%), 100 U/mL penicillin, and 100 μg/mL streptomycin. Cells were treated at passages 3 through 6 and 70% to 80% confluence. To simulate an IRI event, the cells were pretreated with hypoxia (3% O_2) at room temperature for 2 hours. (a) Then, NaHS solution (a common H_2S donor; 10, 30, 50, or 100 μmol/L) was added to the medium of L6 cells in Petri dishes. The cells were subjected to a normoxic (20% O_2) environment at room temperature for 12 hours and then used for assays. (b) For in vitro mechanism experiments, NaHS solution (50 μmol/L) was added to the cell medium with (i) hypotaurine (an H_2S scavenger, 200 mmol/L) or H_2O_2 (100 μmol/L) or (ii) GSK690693 (GSK, a AKT protein phosphorylation inhibitor, 1 μmol/L) or SC79 (SC, a AKT protein phosphorylation agonist, 10 μg/mL). Then, all cells were subjected to normoxia (20% O_2) at room temperature for 12 hours. At the end of the incubation, the cells were used for assays.

2.14 | Histological examinations

Hematoxylin-eosin (H&E) staining and scanning electron microscopy of the macrothrombus and immunohistochemistry staining for CD41, caspase-3, and -9 are described in the Appendix S1.

2.15 | Reactive Oxygen Species detection

A description is provided in the Appendix S1.

2.16 | In vivo and ex vivo apoptosis assays

Cellular apoptosis was determined by terminal deoxynucleotidyl transferase dUTP nick end labeling (TUNEL) staining of rat skeletal muscle and culturing of L6 cells and HUVECs. A description is provided in the Appendix S1.

2.17 | Western blotting

Bcl-2, Bax, caspase-3 and -9, Akt, p-AKT, NQO1, SOD2, and β-actin protein levels were determined by western blotting as previously described.[21] A description is provided in the Appendix S1.

2.18 | SOD and malondialdehyde quantification in skeletal muscle

To detect SOD and malondialdehyde (MDA) in skeletal muscle, tissue was harvested, homogenized, and centrifuged for 15 minutes (3000*g*, 4°C). SOD and MDA were quantitated using commercial kits (Nanjing Jiancheng Bioengineering Institute) according to the manufacturer's protocols.

2.19 | Detection of serum skeletal muscle injury markers and proinflammatory cytokines

Rat plasma creatine kinase (CK), myoglobin (Myo), interleukin-6 (IL-6), and tumor necrosis factor-α (TNF-α) were analyzed. A description is provided in the Appendix S1.

2.20 | Circulatory macrophage isolation and vitality assessment

A description is provided in the Appendix S1.

2.21 | Statistical analysis

Statistical analyses were performed using SPSS 20.0 (SPSS, Inc). Numerical variables are presented as the mean ± standard deviation. Comparisons between multiple groups were analyzed by one-way ANOVA, followed by Bonferroni's multiple comparison test. Mb and hs-Mbs stability data were analyzed by repeated-measures ANOVA. Blood flow velocity data among groups, which were not normally distributed, were analyzed by the nonparametric Kruskal-Wallis H test, followed by Dunn's multiple comparison tests. Fisher's exact test was used to analyze differences in the recanalization rate between groups. $P < .05$ was considered to indicate statistical significance.

3 | RESULTS

3.1 | Characterization of hs-Mbs

Previously characterized stable hs-Mbs with an optimal H_2S/C_3F_8 ratio of 1:1 was used. Both Mbs and hs-Mbs were milk-like in appearance with no macroscopic difference in density (Figure S1A). Under the microscope, both particles were spherical without aggregation, and there was no significant difference in particle size (Figure S1B). Comparable initial concentrations of 0.97 to 1.15 × 10^9/mL ($P > .05$, Figure S1C) and mean diameters of 2.07 to 2.73 μm ($P > .05$, Figure S1D) were observed for both Mbs. hs-Mbs displayed H_2S encapsulation of 0.43 ± 0.05 μmol/mL, and no H_2S loading was detected in Mbs (Figure S1E). The concentration of both hs-Mbs and Mbs remained stable for 72 hours (Figure S1F) under storage condition of 4°C.

3.2 | In vitro H_2S delivery by hs-Mbs+US

US-triggered H_2S release from hs-Mbs was investigated in a flow system that mimics corporeal flow conditions (Figure S1G). The baseline H_2S level fluctuated at 0 μmol/L (Figure S1H). During hs-Mbs infusion, the solution H_2S concentration slightly increased, with a subsequent slow decrease toward 0 μmol/L within 30 seconds. The H_2S concentration increased rapidly within the first 15 seconds of sonication, was maintained at a stable level during sonication, and rapidly decreased to baseline (0 μmol/L) within 15 seconds after stopping US (Figure S1H). The maximum concentration of H_2S was markedly increased under US sonication (Figure S1I). These results demonstrated the feasibility of H_2S release from US-triggered hs-Mbs destruction.

3.3 | Specific in vivo H_2S delivery by hs-Mbs+US and in vivo pharmacokinetics of hs-Mbs

We used CEUS to explore the US-mediated destruction of Mbs and hs-Mbs and subsequent local H_2S delivery in healthy rat hindlimbs. After intravenous infusion, both Mbs and hs-Mbs quickly spread throughout the body, as evidenced by greatly enhanced hindlimb US signal (Figure S1J). Then, the VI immediately and substantially decreased in both groups upon US sonication near the hindlimb (Figure S1J,K), indicating that Mbs and hs-Mbs were quickly fragmented by US sonication. The pharmacokinetic monitor suggested the residence time of the hs-Mbs in the circulation (without US sonication) was 13.8 ± 0.6 minutes (Figure S1L).

To determine specific tissue delivery of H_2S by hs-Mbs destruction, left hindlimb skeletal muscle, liver, and kidney tissues were collected immediately after the cessation of hindlimb US radiation in healthy rats. H_2S levels were considerably increased in hindlimb skeletal muscle in US+hs-Mbs compared with hs-Mbs, whereas there were no significant differences in H_2S levels in the kidney or liver with or without US (Figure 1A). Similarly, in white (Figure 1B) and red (Figure 1C) left iliac artery-thromboembolized rats, H_2S content in rat hindlimb skeletal muscle was significantly increased when hs-Mbs was under US sonication. These results indicated that hs-Mbs could deliver H_2S to specific tissue under focused US radiation.

Next, we demonstrate that H_2S delivery can alleviate cell apoptosis. As described previously, cultured L6 cells were pretreated under hypoxia (3% O_2) for 2 hours. NaHS solution of 10, 30, 50, or 100 μmol/L was then added to the media, respectively, followed by 12 hours of normoxia (20% O_2). TUNEL staining (Figure 1D,E) and flow cytometry (Figure 1F,G) analysis showed a dose-dependent relationship between H_2S concentration and the antiapoptotic effects. The optimum activity of antiapoptosis was observed with 50 μmol/L NaHS solution, and this concentration was used in further studies.

3.4 | In vitro thrombolytic effect of hs-Mbs+US

To detect the thrombolysis efficacy of US+hs-Mbs, we prepared ex vivo white and red macrothrombi and established the thrombolysis setup described previously. H&E staining and scanning electron microscopy imaging showed the white thrombi consisted of a dense fibrin-platelet meshwork and a few erythrocytes (Figure 2A), whereas the red thrombi were composed of compact erythrocytes and a relatively loose fibrin meshwork (Figure 2F). US transverse images showed that the prepared white or red macrothrombi were comparable before treatment (Figure 2B,G). The thrombi were then treated for 30 minutes (Figure 2B,G). The increase in flow velocity and decrease in both thrombotic area percent in transverse sections and clot mass were significantly greater in the Mbs+US and hs-Mbs+US groups than the other two groups, with similar thrombolysis potency between the two Mbs groups (Figure 2C,E and Figure 2H,J). These results showed that the thrombolytic effect of hs-Mb+US was similar with that of Mbs+US for both in vitro macrothrombi.

3.5 | In vivo thrombolytic effect of hs-Mbs+US

We then determined the thrombolysis efficacy of hs-Mbs+US in thromboembolic rat iliac artery. The white macrothrombi contained a dense fibrin-platelet network and the CD41 signal (platelets) was abundant (Figure 3A), whereas the red thrombi consisted of a mass of erythrocytes with scarce CD41 signal (Figure 3F). US imaging showed that both macrothrombi were successfully and comparably induced in iliac artery among four groups (Figure 3B,G). Consistently, CEUS showed a low flow velocity in artery and an obvious absence of perfusion in the rat hindlimb before treatment (Figure 3B,G). After 30 minutes of treatment, the recanalization rate, vessel flow velocity increase, and VI of CEUS imaging were comparable in the Mbs+US and hs-Mbs+US groups for both thromboembolism models and were substantially higher than other groups (Figure 3C-E,H-J). Vessel recanalization was defined as greater than a 20% increase in blood flow compared with the baseline impaired blood flow, and the recanalization rate was defined as the ratio of recanalized samples/total samples × 100%. Our

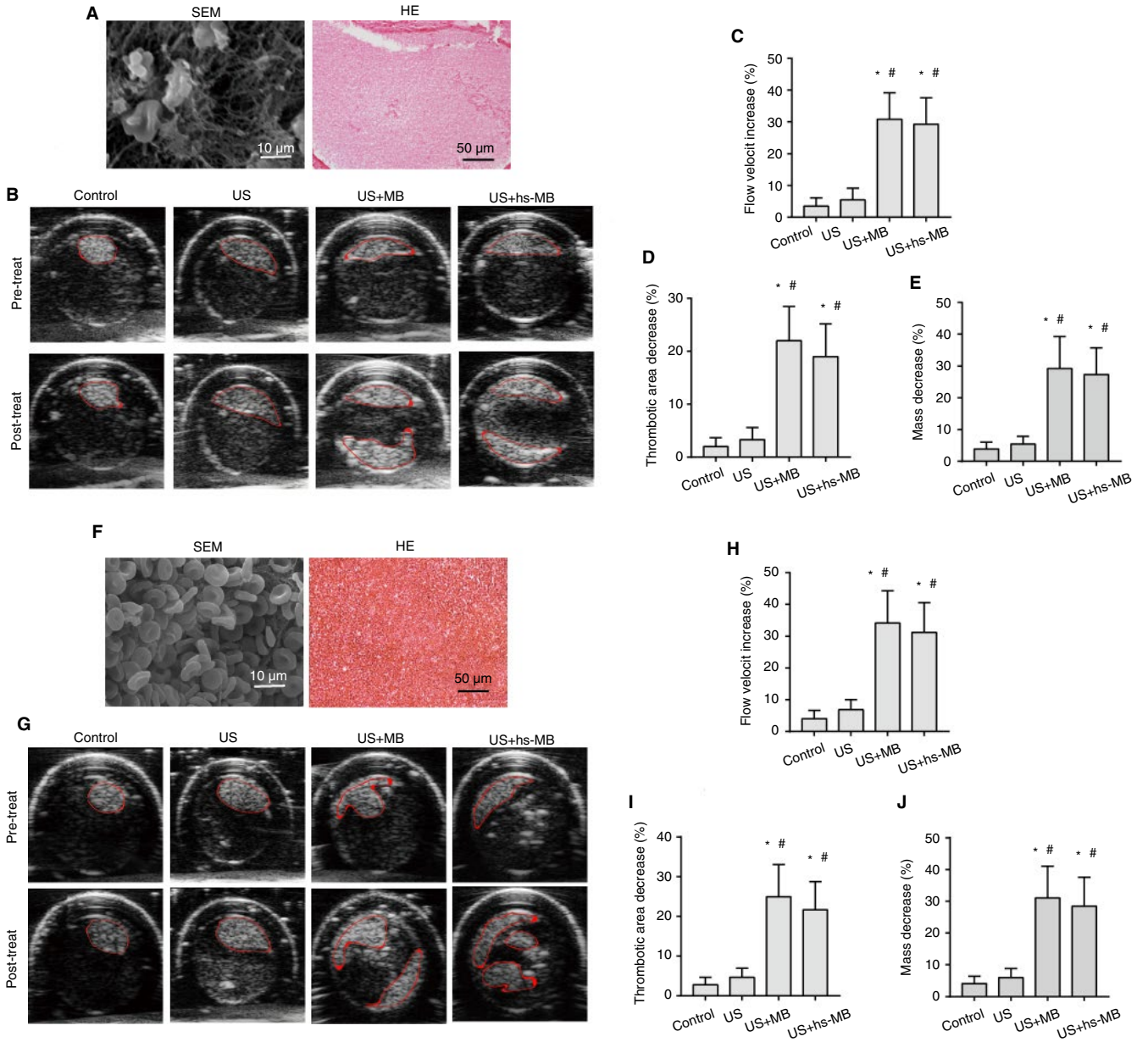

FIGURE 2 Thrombolytic effect of hs-Mbs+US and Mbs+US in ex vivo macrothrombi. (A) H&E staining and scanning electron microscopy (SEM) of in vitro white macrothrombi. (B) White macrothrombi in the transverse view of the rubber tube before and after treatment. Quantification of (C) increased blood flow velocity, (D) thrombus reduction in the transverse section, and (E) decreased clot mass in white macrothrombi after treatment. (F) H&E staining and scanning electron microscopy of in vitro red macrothrombi. (G) Red macrothrombi in the transverse view of the rubber tube before and after treatment. Quantification of (H) increased blood flow velocity, (I) thrombus reduction in the transverse section, and (J) decreased clot mass in red macrothrombi after treatment. Control, controlled saline infusion; US, ultrasound; hs-Mbs, microbubble loaded with hydrogen sulfide. *P < .05 vs control; #P < .05 vs US, n = 15 per group [Color figure can be viewed at wileyonlinelibrary.com]

results indicated that the in vivo thrombolysis of US+hs-Mbs was as effective as that of US+Mbs for both macrothrombi.

3.6 | hs-Mbs+US improve hindlimb function

A hindlimb function was assessed at 7 days after the treatment: both Mbs+US and hs-Mbs+US markedly lowered the ambulatory impairment score compared with other groups, and hs-Mbs+US further reduced the score compared with Mbs+US (Figure 4A,E), suggesting a robust tissue protection against IRI by artery recanalization and H_2S delivery.

3.7 | hs-Mbs+US decreases IRI-induced inflammation and OS

IRI is associated with excessive reactive oxygen species (ROS) generation and tissue inflammation upon the reintroduction of O_2 to

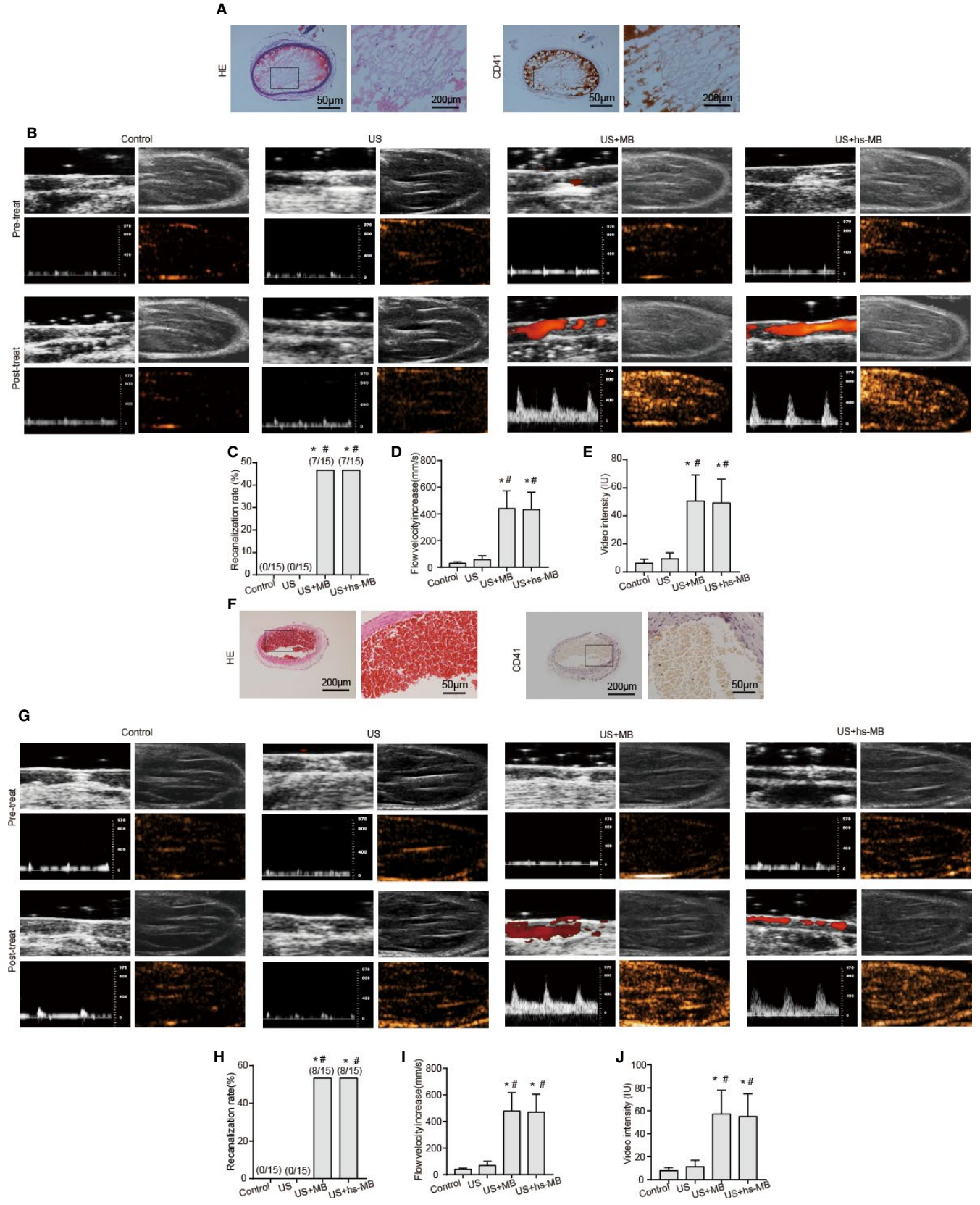

ischemic tissue. IL-6 and TNF-α are potent proinflammatory cytokines. MDA and SOD are accepted biomarkers of pro-OS and antioxidant defense, respectively. We introduced healthy rats as a negative control and occlusion/recanalization rats as a positive control for IRI. As expected, in comparison to non-thromboembolism (normal), occlusion/recanalization (IRI) instigated tissue

FIGURE 3 Thrombolytic effect of hs-Mbs+US and Mbs+US in rat left iliac artery thromboembolism models. (A) Representative images of H&E staining and CD41 immunohistochemical staining of in vivo white thrombi. (B) Diagnostic US imaging of white thrombi and CEUS imaging of hindlimb perfusion before and after treatment. Quantitation of the (C) recanalization rate, (D) blood flow velocity, and (E) video intensity of CEUS imaging after treatment in white thromboembolism models. (F) Representative images of H&E staining and CD41 immunohistochemical staining of in vivo red thrombi. (G) Diagnostic US imaging of red thrombi and CEUS imaging of hindlimb perfusion before and after treatment. Quantitation of the (H) recanalization rate, (I) blood flow velocity, and (J) video intensity of CEUS imaging after treatment in red thromboembolism models. Control, controlled saline infusion; US, ultrasound; hs-Mbs, microbubble loaded with hydrogen sulfide. *P < .05 vs control; #P < .05 vs US, n = 15 per group. [Color figure can be viewed at wileyonlinelibrary.com]

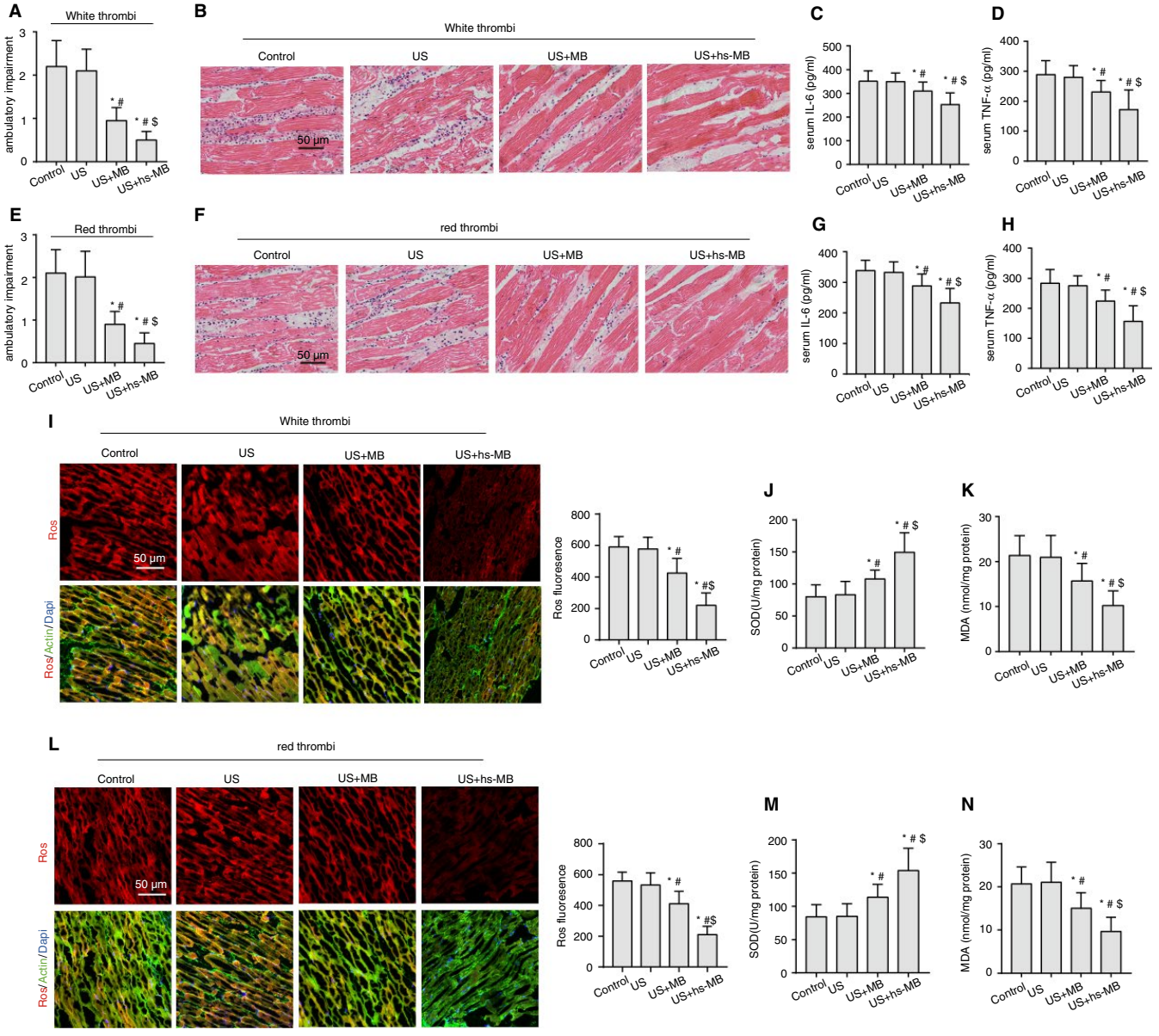

FIGURE 4 In vivo mitigation of IRI-induced skeletal muscle oxidative stress and inflammation by hs-Mbs+US. (A) Ambulatory impairment score of white thrombus model rats left hindlimb a week after the treatment. (B) H&E staining of white thrombus model rats hindlimb skeletal muscle after different treatments. Serum (C) IL-6 and (D) TNF-α in white thrombus model rats after treatments. (E) Ambulatory impairment score of red thrombus model rats left hindlimb a week after the treatment. (F) H&E staining of red thrombus model rats hindlimb skeletal muscle after different treatments. Serum (G) IL-6 and (H) TNF-α in white red model rats after treatments. (I) Representative immunofluorescence images of ROS-stained skeletal muscle sections from rats hindlimb with white thrombi. (J) SOD and (K) MDA levels in rat skeletal muscle with white thrombi after different treatments. (L) Representative immunofluorescence images of ROS-stained skeletal muscle sections from rats hindlimb with red thrombi. (M) SOD and (N) MDA levels in rat skeletal muscle with red thrombi after different treatments. Control, controlled saline infusion; US, ultrasound; hs-MB, microbubble loaded with hydrogen sulfide. *P < .05 vs control; #P < .05 vs US, $$P$ < .05 vs US+MB, n = 15 per group [Color figure can be viewed at wileyonlinelibrary.com]

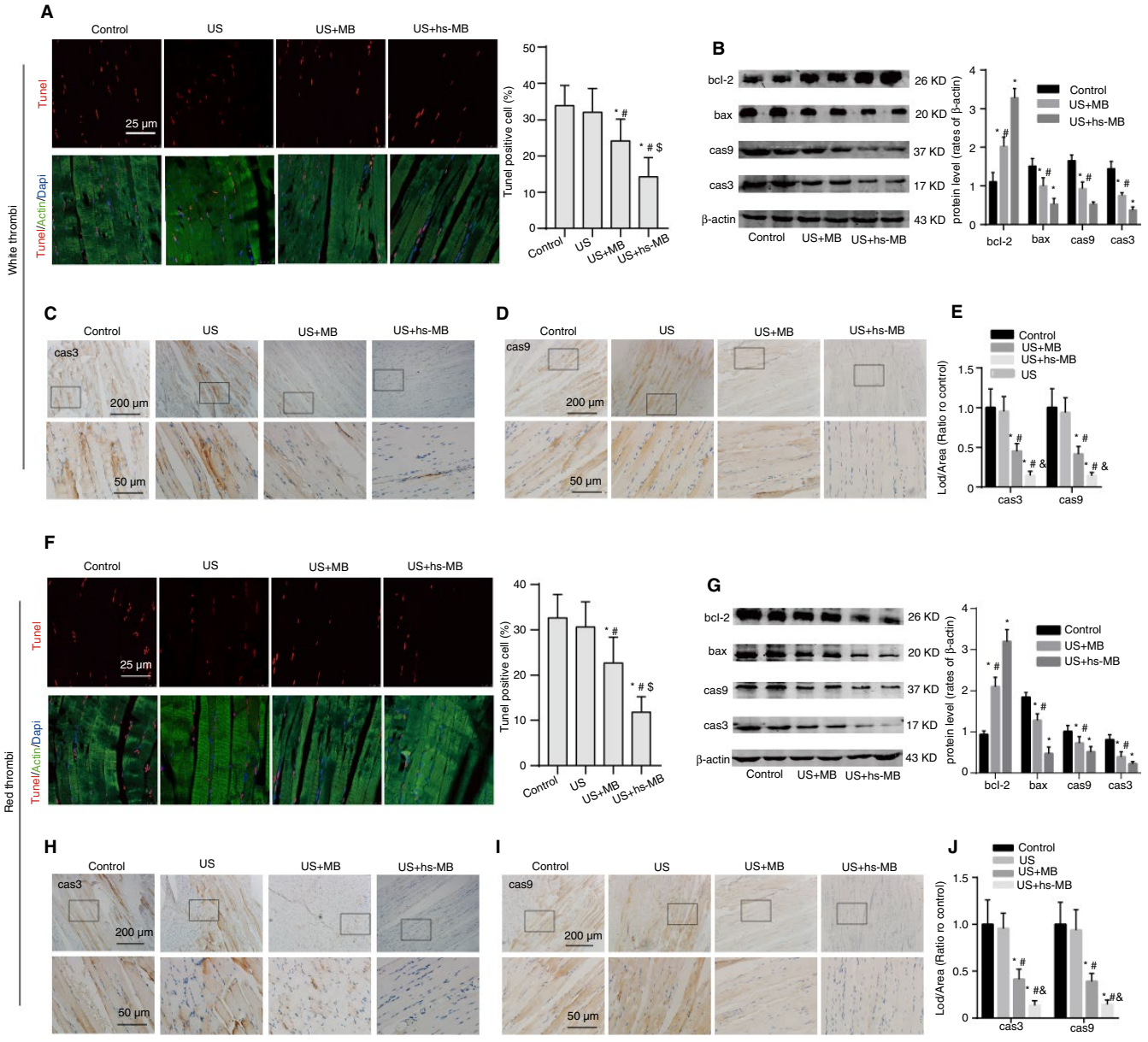

FIGURE 5 In vivo alleviation of IRI-induced skeletal muscle cell apoptosis by hs-Mbs+US. (A) Representative immunofluorescence images and quantification of TUNEL-stained skeletal muscle sections from rats in the white left iliac artery macrothrombus model. (B) Representative Western blotting images and statistical analysis of Bcl-2, Bax, caspase-9, and caspase-3 in rat skeletal muscle in the white thrombus model. Representative (C) immunohistochemical staining for caspase-3, (D) caspase-9, and (E) quantification in the white thrombus model. (F) Representative immunofluorescence images and quantification of TUNEL-stained skeletal muscle sections from rats in the red left iliac artery macrothrombus model. (G) Representative Western blotting images and statistical analysis of Bcl-2, Bax, caspase-9, and caspase-3 in rat skeletal muscle in the red thrombus model. Representative (H) immunohistochemical staining for caspase-3, (I) caspase-9, and (J) quantification in the red thrombus model. Control, controlled saline infusion; US, ultrasound; hs-Mbs, microbubble loaded with hydrogen sulfide. *P < .05 vs control; #P < .05 vs US, $$P$ < .05 vs Mbs+US, n = 15 per group [Color figure can be viewed at wileyonlinelibrary.com]

leukocyte infiltration (Figure S2B), leveled serum TNF-α and IL-6 (Figure S2C,D) and tissue ROS and MDA contents, alleviated tissue SOD (Figure S2E-H), and promoted cell apoptosis as indicated by increased TUNEL staining and apoptotic caspase-3 and caspase-9 (Figure S2I-M). Furthermore, serum skeletal muscle injury markers of CK and Myo were significantly elevated in the IRI group (Figure S3A,B).

In both white and red thrombus-associated IRI, hs-Mbs+US significantly ameliorated leukocyte infiltration to tissue (Figure 4B,F) and decreased plasma IL-6 and TNF-α (Figure 4C,D,G,H) compared with the rest of groups (P < .05). Additionally, hs-Mbs+US markedly decreased the skeletal muscle ROS (Figure 4I,L) and plasma MDA, and increased plasma SOD (Figure 4J,K,M,N), indicating an amelioration of OS and inflammation by US+hs-Mbs.

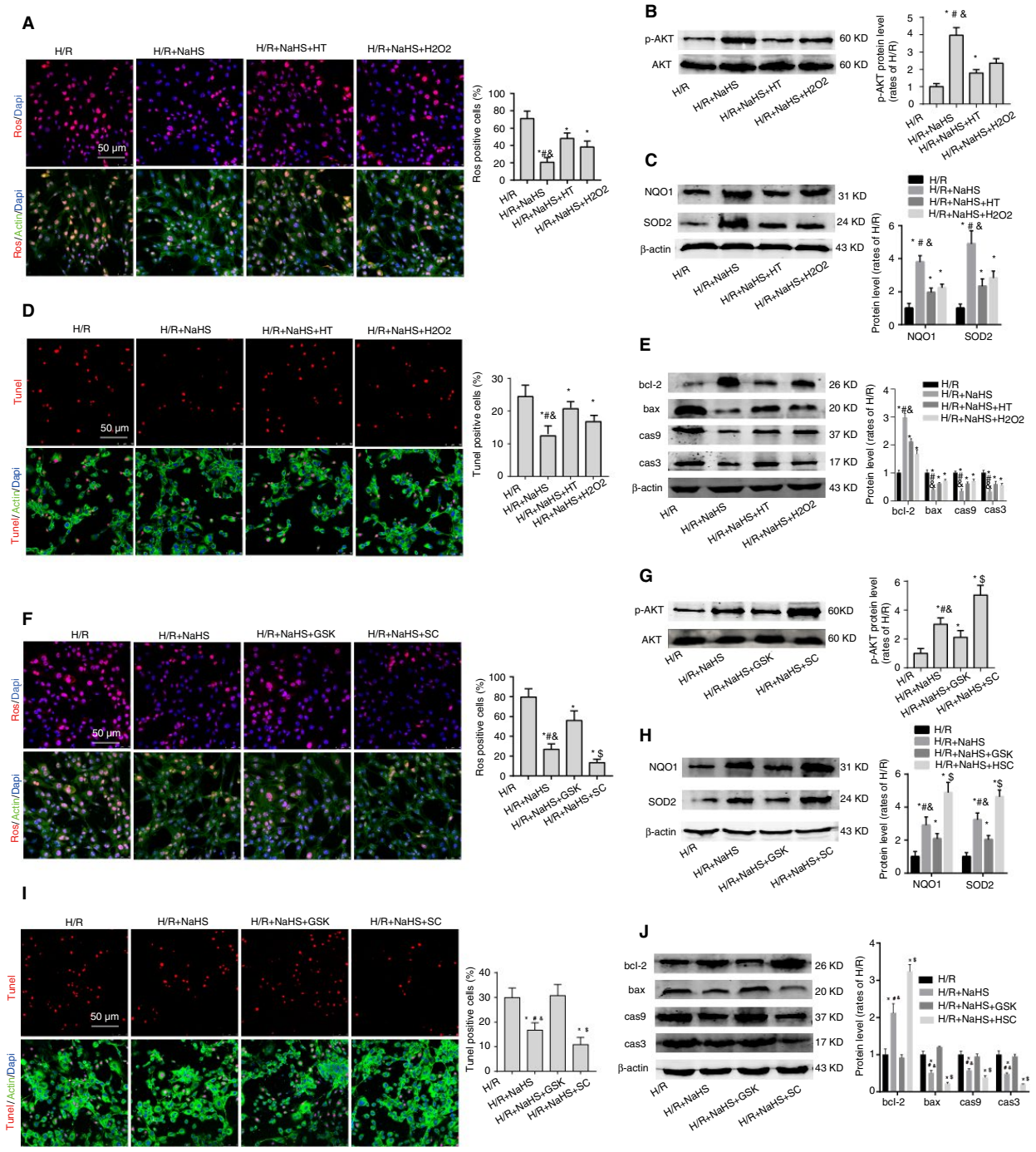

FIGURE 6 In vitro therapeutic effect of NaHS on hypoxia/reoxygenation L6 cells. L6 cells were pretreated with hypoxia (3% O_2) for 2 h, treated with various solutions, and then subjected to normoxia (20% O_2) for 12 h. (A) Representative immunofluorescence images of cellular ROS and statistical analysis. (B) Protein expression of total and phosphorylated AKT in L6 cells and statistical analysis. (C) Protein expression of NQO1 and SOD2 in L6 cells and statistical analysis. (D) Representative immunofluorescence images of TUNEL-stained sections of L6 cells and statistical analysis. (E) Protein expression of Bcl-2, Bax, caspase-9, and caspase-3 in L6 cells and statistical analysis. *P < .05 vs the H/R group; #P < .05, H/R+NaHS vs H/R+NaHS+HT; &P < .05, H/R+NaHS vs H/R+NaHS+H_2O_2. (F) Representative immunofluorescence images of cellular ROS and statistical analysis. (G) Protein expression of total and phosphorylated AKT in L6 cells with various treatments and statistical analysis. (H) Protein expression of NQO1 and SOD2 in L6 cells and statistical analysis. (I) Representative immunofluorescence images of TUNEL-stained sections of L6 cells and statistical analysis. (J) Protein expression of Bcl-2, Bax, caspase-9, and caspase-3 in L6 cells and statistical analysis. NaHS, sodium hydrosulfide; HT, hypotaurine, an H_2S scavenger; H_2O_2, hydrogen peroxide, stimulus production of ROS. GSK690693 (GSK), AKT protein phosphorylation inhibitor; SC79, AKT protein phosphorylation agonist. *P < .05 vs the H/R group; #P < .05 vs H/R+NaHS+GSK690693; &P < .05 vs H/R+NaHS+SC79; $$P$ < .05+vs H/R+NaHS+GSK690693 [Color figure can be viewed at wileyonlinelibrary.com]

3.8 | hs-Mbs+US alleviates IRI-induced apoptosis

We then explored whether the ability of hs-Mbs+US to protect against IRI is relevant to reducing apoptosis. There was a substantial decrease in the total number of TUNEL-positive nuclei in the hs-Mbs+US group (14.26 ± 5.25 and 11.83 ± 3.41 in white and red thrombus model, respectively) compared with the Mbs+US group (24.15 ± 5.94 in white thrombus model and 22.71 ± 5.70 in red thrombus model; $P < .05$, respectively), US group (32.01 ± 6.581 in white thrombus model and 30.64 ± 5.522 in red thrombus model; $P < .05$, respectively), and control group (33.85 ± 5.59 in white thrombus model and 32.64 ± 5.20 in red thrombus model; $P < .05$, respectively), and a lower ratio of TUNEL-positive nuclei in the Mbs+US group than in the control groups ($P < .05$, respectively, Figure 5A,F). We found that the protein levels of the pro-apoptosis biomarkers Bax, caspase-3, and caspase-9 were significantly lower, whereas Bcl-2 were significantly higher in the hs-Mbs+US group than the Mbs+US and control groups (Figure 5B,G). Immunohistochemistry analysis confirmed the trend in caspase-3 and caspase-9 protein expression (Figure 5C-E,H-J). Besides, in both thrombus models, the plasma concentrations of CK and MYO were significantly reduced in the hs-Mbs+US compared with the control, US and Mbs+US (Figure S3C,D). Of note, compared with the positive IRI control, Mbs+US had comparable effects in alleviating tissue OS, apoptosis, and the inflammatory response.

Taken together, our results indicated that H_2S delivery by hs-Mbs+US conferred alleviation of IRI-induced muscle injury and improved hindlimb function.

3.9 | In vitro H_2S reduces apoptosis by decreasing ROS and activating the Akt pathway

Next, we explored the potential mechanism by which H_2S reduced IRI. L6 cells and HUVECs were pretreated with hypoxia followed by exposure to normal saline (control [H/R] group), NaHS (H/R+NaHS), NaHS and an H_2S scavenger (H/R+NaHS+HT), or NaHS and H_2O_2 (H/R+NaHS+H_2O_2), and then subjected to normoxia for 12 hours. Compared with H/R, NaHS significantly decreased cell ROS content and increased Akt phosphorylation and antioxidative NQO1 and SOD2 levels (Figure 6A-C). NaHS also decreased the numbers of TUNEL-positive cells (Figure 6D) and apoptotic Bax, caspase-3, and -9 protein levels (Figure 6E), and increased anti-apoptotic Bcl-2. These results suggested the anti-oxidative and antiapoptotic effects of NaHS, and these protective effects could be largely reversed by hypotaurine (Figure 6A-E).

Studies have reported that ROS induce cell apoptosis by inactivating Akt phosphorylation, thus decreasing the activity of downstream Bcl-2 and enhancing the activity of Bax, caspase-3, and caspase-9. To determine whether the antioxidative and anti-apoptosis effects of H_2S were partly mediated by activation of the Akt pathway, we used the Akt phosphorylation inhibitor GSK6900693 (H/R+NaHS+GSK6900693) or promoter SC79 (H/R+NaHS+SC79) to modulate p-Akt expression. Akt phosphorylation was altered as expected by GSK6900693 and SC79 (Figure 6G). The anti-OS and anti-apoptosis effects of NaHS were further augmented by SC79 or substantially reversed by GSK6900693, indicating that H_2S conferred anti-OS and anti-apoptosis effects by altering Akt pathways (Figure 6F-J). Similar trends of these protection were observed in cultured HUVECs (Figure S4A,B). To summarize, we demonstrated that H_2S conferred protection against OS and apoptosis in IRI through the Akt pathway.

3.10 | hs-Mbs+US do not affect hemodynamics, respiration, or blood macrophage vitality

To evaluate the safety of US+hs-Mbs, we monitored blood pressure, heart rate, and respiratory rate during and 10 minutes after various treatments in the white thrombus model. There were no significant changes in these parameters among the groups (Table S1). We also found no significant difference in macrophage vitality in the four groups after the treatment (Figure S5A,B), implying that 30 minutes of US+hs-Mbs did not cause damage to circulatory macrophages. To summarize, our results indicated that US+hs-Mbs were safe without obvious systemic side effects.

4 | DISCUSSION

In the present study, we demonstrated that integrated hs-Mbs+US effectively dissolve both white and red macrothrombi and simultaneously protect against skeletal muscle IRI. Compared with Mbs+US, hs-Mbs+US evoked similar thrombolysis and improvement in hindlimb blood perfusion but greater alleviation of skeletal muscle IRI. We demonstrated that this additional alleviation was mediated by the release of H_2S via US-triggered hs-Mbs destruction and might be associated with the anti-apoptosis, antiOS, and anti-inflammatory functions of H_2S. This integrated treatment may be a promising adjunct, or even alternative, to the current routine therapy for vessel recanalization and IRI prevention.

We found that hs-Mbs+US had a substantial thrombolysis effect in large vessels, which was noninferior to that of Mbs+US, as evidenced by the similar recanalization rate, increase in blood flow velocity, and hindlimb perfusion. Mechanistically, Mbs-enhanced sonothrombolysis is largely dependent on the acoustic cavitation of Mbs, which is determined by the Mbs concentration and performance.[34] The performance of Mbs is influenced by their structure, size, and stability in solution or blood flow, which are in turn determined by the shell material, gas contained within the bubble, and bubble size distribution.[34] The concentration and particle diameter of our prepared hs-Mbs were comparable to those of control Mbs. Moreover, Mbs and hs-Mbs share the same phospholipid shell, which may lead to comparable acoustic dissolution and fragmentation propensity under identical US conditions.[35] The only difference between the two particles was the loaded gas core. Although H_2S is an active and unstable gas when dissolved and may impair the stability

of hs-Mbs, the large and inert molecule C_3F_8 (C_3F_8:H_2S = 1:1) was introduced as an internal gas to stabilize hs-Mbs, which was successful in a previous study.[23] Others have similarly found that the inclusion of C_3F_8 markedly enhances the stability of Mbs loaded with O_2 or NO.[36-38] More importantly, we observed no obvious alterations in hs-Mbs solution concentration during the 72-hour storage, supporting the good stability of hs-Mbs. Thus, it is reasonable to conclude that the partial introduction of H_2S in the core of C_3F_8 Mbs (hs-Mbs) does not significantly impact the thrombolytic effect, as does the full C_3F_8 core (Mbs) under the same US conditions.

Next, we investigated the efficiency and safety of H_2S release by US-triggered hs-Mbs destruction and the specific bioavailability of H_2S to IRI tissue. In the artificial flow system, 1.9 MHz of diagnostic US was sufficient to cause rapid H_2S accumulation in solution; H_2S levels reached a plateau within 15 seconds and remained stable throughout the sonication, indicating the high efficiency and stability of H_2S release. The H_2S concentration promptly declined to the baseline level in solution within 15 seconds after stopping the US treatment, indicating hs-Mbs were sufficiently stable to avoid significant H_2S release in the absence of US. In the rat hindlimb macrothrombus model, the CEUS signal showed instant hs-Mbs movement to skeletal muscle via circulation and destruction by US in situ. In healthy rats, 30 minutes of hindlimb US+hs-Mbs led to significantly higher H_2S content in hindlimb skeletal muscle, but not in kidney and liver, suggesting the specific delivery of H_2S to targeted tissue. Additionally, hs-Mbs+US had no obvious effect on hemodynamic indicators and blood macrophages. These results indicated that hs-Mbs+US were an efficient and safe strategy for organ-specific H_2S delivery.

More importantly, we found that US+hs-Mbs could simultaneously relieve skeletal muscle IRI and improve hindlimb muscle function through the synergistic network of anti-apoptosis, antioxidative, and anti-inflammation. Apoptosis has been proposed as a key mediator and major manifestation of IRI-induced damage.[39] In vitro, there was a dose-effect relationship between NaHS concentration and the antiapoptosis in hypoxia/reoxygenation cells, suggesting a causal impact of H_2S on alleviating cellular apoptosis. In vivo and in vitro, US+hs-Mbs or NaHS significantly decreased TUNEL-positive nuclei and the levels of the proapoptotic Bax, caspase-3, and caspase-9, whereas significantly increased the antiapoptotic Bcl-2 levels in skeletal muscle or L6 cells. In rescue experiments, the anti-apoptosis effect of NaHS was largely neutralized by a H_2S scavenger or Akt phosphorylation inhibitor but was enhanced by an Akt phosphorylation agonist, supporting the hypothesis that H_2S-mediated Akt activation is crucial for ameliorating cellular apoptosis during IRI. The occurrence of IRI is closely associated with ROS generation and subsequent damages such as cell injury and apoptosis.[40] In our study, ROS levels from skeletal tissue were significantly reduced, whereas the antioxidant enzyme SOD was substantially upregulated in the US+hs-Mbs compared with the Mbs+US group. These results are in accordance with the existing notion that H_2S is a potent antioxidant that prevents ROS generation, scavenges ROS, and strengthens endogenous antioxidant systems such as SOD. We observed significantly less leukocytes infiltration into hindlimb skeletal muscle and lower plasma IL-6 and TNF-α in the US+hs-Mbs group than in other groups, suggesting that H_2S is anti-inflammatory. IL-6 is released upon IR damage and increases neutrophil adhesion and inflammatory responses,[41] and TNF-α plays multiple roles in the pathogenesis of IRI by favoring neutrophil infiltration, enhancing ROS production, and promoting inhibitory and apoptotic cell activity.[42] In agreement with our results, a previous study has shown that H_2S decreases the leukocyte population within the ischemic zone of myocardial tissue during IRI. SPRC, a H_2S donor, attenuates lipopolysaccharide-induced TNF-α expression to produce an anti-inflammatory effect in H9C2 cells.[42] Taken together, H_2S is capable of potently alleviating IRI through synergistic mechanisms.

There are several limitations of our study. First, although we found the alleviation of tissue IRI by hs-Mbs+US was associated with antiapoptosis, antioxidant stress, and anti-inflammation, the specific molecular signaling network involved remains to be identified. Second, because we have demonstrated the protection against tissue IRI by in situ release of H_2S from hs-Mbs+US and that our magnitude of tissue H_2S level have also been reported by others to be associated with organ protection,[23,43] hs-Mbs+US should have potential and opportunity in future clinical IRI protection. However, a series of questions remain to be answered before its final clinical practice. In the current study, we gained organ IRI protection using hs-Mbs infusion (1×10^9 Mbs/mL) with 30 minutes of US sonication, but whether this protection is in a dose- and time-dependent manner merits deeper exploration. In addition, other factors as to gas-loading capacity of Mbs, Mbs administration pattern, US parameters, and so on all influence the H_2S accessibility to organ and final anti-IRI effects of hs-Mbs+US. Accordingly, further studies should be warranted for investigation of hs-Mbs+US in potential clinical translation.

In conclusion, hs-Mbs+US are efficacious at dissolving macrothrombi and simultaneously protecting against organ IRI by in situ H_2S delivery via US-targeted Mbs destruction. This protection may be associated with the anti-apoptosis, anti-OS, and anti-inflammatory functions of H_2S. hs-Mbs+US treatment may represent a novel integrated strategy to treat thromboembolism and subsequent IRI.

CONFLICT OF INTEREST

The manuscript has been read and approved for submission by all authors. They declare no conflicts of interest.

AUTHOR CONTRIBUTIONS

Jiayuan Zhong actually, Yili Sun, and Yuan Han were pivotal in the design and implementation of the experiments and interpretation of results. Xiaoqiang Chen and Hairui Li provided technical suggestions. Yusheng Ma and Yanxian Lai conducted the statistical analyses. Guoquan Wei, Xiang He, and Mengsha Li drafted the manuscript and edited the paper. Wangjun Liao, Yulin Liao, Shiping Cao, and Jianping Bin guided the research design and interpretation of the results and supervised the study.

REFERENCES

1. Wendelboe AM, Raskob GE. Global burden of thrombosis: epidemiologic aspects. *Circ Res*. 2016;118(9):1340-1347.
2. Kim JT, Fonarow GC, Smith EE, et al. Treatment with tissue plasminogen activator in the golden hour and the shape of the 4.5-hour time-benefit curve in the National United States Get With the Guidelines-Stroke population. *Circulation*. 2017;135(2):128-139.
3. Zerna C, Siepmann T, Barlinn K, et al. Association of time on outcome after intravenous thrombolysis in the elderly in a telestroke network. *J Telemed Telecare*. 2016;22(1):18-24.
4. Eltzschig HK, Eckle T. Ischemia and reperfusion–from mechanism to translation. *Nat Med*. 2011;17(11):1391-1401.
5. Jennings RB. Historical perspective on the pathology of myocardial ischemia/reperfusion injury. *Circ Res*. 2013;113(4):428-438.
6. Yellon DM, Hausenloy DJ. Myocardial reperfusion injury. *N Engl J Med*. 2007;357(11):1121-1135.
7. Heusch G. Critical issues for the translation of cardioprotection. *Circ Res*. 2017;120(9):1477-1486.
8. Heusch G. Cardioprotection research must leave its comfort zone. *Eur Heart J*. 2018;39(36):3393-3395.
9. Davidson SM, Ferdinandy P, Andreadou I, et al. Multitarget strategies to reduce myocardial ischemia/reperfusion injury: JACC review topic of the week. *J Am Coll Cardiol*. 2019;73(1):89-99.
10. Hausenloy DJ, Botker HE, Engstrom T, et al. Targeting reperfusion injury in patients with ST-segment elevation myocardial infarction: trials and tribulations. *Eur Heart J*. 2017;38(13):935-941.
11. Bos EM, Wang R, Snijder PM, et al. Cystathionine gamma-lyase protects against renal ischemia/reperfusion by modulating oxidative stress. *J Am Soc f Nephrol: JASN*. 2013;24(5):759-770.
12. Calvert JW, Elston M, Nicholson CK, et al. Genetic and pharmacologic hydrogen sulfide therapy attenuates ischemia-induced heart failure in mice. *Circulation*. 2010;122(1):11-19.
13. Fu Z, Liu X, Geng B, Fang L, Tang C. Hydrogen sulfide protects rat lung from ischemia-reperfusion injury. *Life Sci*. 2008;82(23–24):1196-1202.
14. Yin J, Tu C, Zhao J, et al. Exogenous hydrogen sulfide protects against global cerebral ischemia/reperfusion injury via its anti-oxidative, anti-inflammatory and anti-apoptotic effects in rats. *Brain Res*. 2013;1491:188-196.
15. Wang D, Ma Y, Li Z, et al. The role of AKT1 and autophagy in the protective effect of hydrogen sulphide against hepatic ischemia/reperfusion injury in mice. *Autophagy*. 2012;8(6):954-962.
16. Caliendo G, Cirino G, Santagada V, Wallace JL. Synthesis and biological effects of hydrogen sulfide (H2S): development of H2S-releasing drugs as pharmaceuticals. *J Med Chem*. 2010;53(17):6275-6286.
17. Zhao Y, Biggs TD, Xian M. Hydrogen sulfide (H2S) releasing agents: chemistry and biological applications. *Chem Commun (Camb)*. 2014;50(80):11788-11805.
18. Polhemus D, Kondo K, Bhushan S, et al. Hydrogen sulfide attenuates cardiac dysfunction after heart failure via induction of angiogenesis. *Circ Heart Fail*. 2013;6(5):1077-1086.
19. Gan X, Su G, Zhao W, Huang P, Luo G, Hei Z. The mechanism of sevoflurane preconditioning-induced protections against small intestinal ischemia reperfusion injury is independent of mast cell in rats. *Mediators Inflamm*. 2013;2013:378703.
20. Unger E, Porter T, Lindner J, Grayburn P. Cardiovascular drug delivery with ultrasound and microbubbles. *Adv Drug Deliv Rev*. 2014;72:110-126.
21. Tong J, Ding J, Shen X, et al. Mesenchymal stem cell transplantation enhancement in myocardial infarction rat model under ultrasound combined with nitric oxide microbubbles. *PLoS One*. 2013;8(11):e80186.
22. McEwan C, Owen J, Stride E, et al. Oxygen carrying microbubbles for enhanced sonodynamic therapy of hypoxic tumours. *J Control Release: Off J Control Release Soc*. 2015;203:51-56.
23. Chen G, Yang L, Zhong L, et al. Delivery of hydrogen sulfide by ultrasound targeted microbubble destruction attenuates myocardial ischemia-reperfusion injury. *Sci Rep*. 2016;6:30643.
24. Xie F, Slikkerveer J, Gao S, et al. Coronary and microvascular thrombolysis with guided diagnostic ultrasound and microbubbles in acute ST segment elevation myocardial infarction. *J Am Soc Echocardiogr: Off Publ Am Soc Echocardiogr*. 2011;24(12):1400-1408.
25. Culp WC, Erdem E, Roberson PK, Husain MM. Microbubble potentiated ultrasound as a method of stroke therapy in a pig model: preliminary findings. *J Vasc Intervent Radiol: JVIR*. 2003;14(11):1433-1436.
26. Culp WC, Porter TR, Lowery J, Xie F, Roberson PK, Marky L. Intracranial clot lysis with intravenous microbubbles and transcranial ultrasound in swine. *Stroke*. 2004;35(10):2407-2411.
27. Birnbaum Y, Luo H, Nagai T, et al. Noninvasive in vivo clot dissolution without a thrombolytic drug: recanalization of thrombosed iliofemoral arteries by transcutaneous ultrasound combined with intravenous infusion of microbubbles. *Circulation*. 1998;97(2):130-134.
28. Nishioka T, Luo H, Fishbein MC, et al. Dissolution of thrombotic arterial occlusion by high intensity, low frequency ultrasound and dodecafluoropentane emulsion: an in vitro and in vivo study. *J Am Coll Cardiol*. 1997;30(2):561-568.
29. Lu Y, Wang J, Huang R, et al. Microbubble-mediated sonothrombolysis improves outcome after thrombotic microembolism-induced acute ischemic stroke. *Stroke*. 2016;47(5):1344-1353.
30. Li H, Lu Y, Sun Y, et al. Diagnostic ultrasound and microbubbles treatment improves outcomes of coronary no-reflow in canine models by sonothrombolysis. *Crit Care Med*. 2018;46(9):e912-e920.
31. Borden MA, Martinez GV, Ricker J, et al. Lateral phase separation in lipid-coated microbubbles. *Langmuir: ACS J Surf Colloids*. 2006;22(9):4291-4297.
32. Huang P, Chen S, Wang Y, et al. Down-regulated CBS/H2S pathway is involved in high-salt-induced hypertension in Dahl rats. *Nitric Oxide: Biol Chem*. 2015;46:192-203.
33. Roessler FC, Ohlrich M, Marxsen JH, et al. The platelet-rich plasma clot: a standardized in-vitro clot formation protocol for investigations of sonothrombolysis under physiological flows. *Blood Coagulat Fibrinol: Int J Haemost Thromb*. 2011;22(5):407-415.
34. de Saint Victor M, Crake C, Coussios CC, Stride E. Properties, characteristics and applications of microbubbles for sonothrombolysis. *Exp Opin Drug Deliv*. 2014;11(2):187-209.
35. Borden MA, Kruse DE, Caskey CF, Zhao S, Dayton PA, Ferrara KW. Influence of lipid shell physicochemical properties on ultrasound-induced microbubble destruction. *IEEE Trans Ultrason Ferroelectr Freq Control*. 2005;52(11):1992-2002.
36. Eisenbrey JR, Albala L, Kramer MR, et al. Development of an ultrasound sensitive oxygen carrier for oxygen delivery to hypoxic tissue. *Int J Pharm*. 2015;478(1):361-367.
37. Kwan JJ, Kaya M, Borden MA, Dayton PA. Theranostic oxygen delivery using ultrasound and microbubbles. *Theranostics*. 2012;2(12):1174-1184.
38. Sutton JT, Raymond JL, Verleye MC, Pyne-Geithman GJ, Holland CK. Pulsed ultrasound enhances the delivery of nitric oxide from bubble liposomes to ex vivo porcine carotid tissue. *Int J Nanomed*. 2014;9:4671-4683.
39. Jose Corbalan J, Vatner DE, Vatner SF. Myocardial apoptosis in heart disease: does the emperor have clothes? *Basic Res Cardiol*. 2016;111(3):31.
40. Duehrkop C, Rieben R. Ischemia/reperfusion injury: effect of simultaneous inhibition of plasma cascade systems versus specific complement inhibition. *Biochem Pharmacol*. 2014;88(1):12-22.
41. Hennein HA, Ebba H, Rodriguez JL, et al. Relationship of the proinflammatory cytokines to myocardial ischemia and dysfunction after uncomplicated coronary revascularization. *J Thorac Cardiovasc Surg*. 1994;108(4):626-635.

42. Pan LL, Liu XH, Gong QH, Zhu YZ. S-Propargyl-cysteine (SPRC) attenuated lipopolysaccharide-induced inflammatory response in H9c2 cells involved in a hydrogen sulfide-dependent mechanism. *Amino Acids*. 2011;41(1):205-215.
43. Huang P, Shen ZZ, Liu J, et al. Hydrogen sulfide inhibits high-salt diet-induced renal oxidative stress and kidney injury in dahl rats. *Oxid Med Cell Longev*. 2016;2016:2807490.

How to cite this article: Zhong J, Sun Y, Han Y, et al. Hydrogen sulfide-loaded microbubbles combined with ultrasound mediate thrombolysis and simultaneously mitigate ischemia-reperfusion injury in a rat hindlimb model. *J Thromb Haemost*. 2021;19:738–752. https://doi.org/10.1111/jth.15110

SUPPORTING INFORMATION

Additional supporting information may be found online in the Supporting Information section.